Benha Journal of Applied Sciences (BJAS) **print: ISSN 2356–9751**
Vol. (8) Issue (5) (2023), (191-210) **online: ISSN 2356–976x**
http://bjas.journals.ekb.eg

Geochemical Characteristics of the Syn-Tectonic Granitoids along Wadi El-Sheikh Area, South Sinai, Egypt.

Walaa Mahmoud Saad and Moustafa Mohamed Moghed
Geology Department, Faculty of Science, Benha University
Corresponding author: walaa.mahmoud@fsc.bu.edu.eg

Abstract

The Wadi El-Sheikh area is situated in south Sinai, and is distinguished by a high abundance of calc-alkaline and alkaline/peralkaline granitoid rocks, as well as related volcanics. These granitoid rocks are of particular geodynamic significance because they contribute to better understanding of how the continental crust of the Arabian Nubian Shield (ANS) formed. Thus, the present study introduces new comprehensive geological field studies, petrological data, and whole rock geochemical data of syn-tectonic granitoids along Wadi El-Sheikh. The composition of the syn-tectonic granitoids (SNG) ranges from quartz-diorite, tonalite, to granodiorite. Geochemically, these SNGs are mainly metaluminous, calc-alkaline, I-type, and correspond to syn-collision volcanic arc granitoids. The investigated syn-tectonic granitoids have high (Al_2O_3/TiO_2) ratios (17.85–80.70), rising toward the higher silica granitoid type (granodiorite), while they also show high (CaO/Na_2O) ratios (0.33–1.44) representing a decrease from quartz-diorite to granodiorite. These characters indicate that the emplacements of SNG were greatly influenced by the magma mixing of mafic and felsic melts. The analyzed granitoids originated at temperatures ranging from 650°C to 700°C and water pressures ranging from 0.5 to 10 kbar. According to the depth of magma segregation, and they were produced at depths of more than 30 km of the lower crust. The considered SNG are commonly concerned with enrichment of LILE and LREE and depletion of HFSE in comparison to N-MORB values (negative Ta and Nb anomalies).

Key words: Wadi El-Sheikh, Syn-tectonic granitoids, Arabian Nubian Shield (ANS), geochemical investigations.

1. Introduction

In Sinai, the crystalline Precambrian rocks occupy a special tectonic belt within the northern part of the Arabian Nubian Shield (ANS). The shield was created as a juvenile crust through the Pan-African orogeny [1, 2& 3]. The current studies indicate the existence of earlier rocks (i.e., rift-related rock that intruded through the separation of the Rodinia [4, 5& 6]. The syn-tectonic granitic rocks were formed during the pre-collision phases of the Neoproterozoic. South Sinai has a widespread distribution of syn-orogenic and late-to-post-orogenic granitoids [7, 8, 9& 10]. At the end of the Pan-African Orogeny (650–550 Ma), syn-orogenic calc-alkaline magmatism representing subduction and collision events was followed by post-collisional magmatism that produced high-K calc-alkaline, alkaline, and peralkaline rocks [11& 12]. The syn-tectonic, calc-alkaline quartz-diorite, tonalite, trondhjemite, granodiorite, and granite intrusions are conformable with the earlier stage (750-610 Ma, [13]). They were created by partial melting of a mantle wedge with little or no crustal contamination [14] or in an ensimatic island arc setting [15& 16]. [16] considered the oldest granitoids of south Sinai to be plutonic rocks of the island arc stage (950 – 650 Ma). [17] used K– Ar techniques to date several of the older granitoids, including diorite, tonalite, and granodiorite, in southwestern Sinai and gave ages ranging from 653±26 to 567±22. According to K-Ar dating, the metagabbro-diorite masses in southwest Sinai were formed during a stage of emplacement and crystallization about 794 Ma, while the thermal event occurred between 690 and 667 Ma [18]. The present study focuses on identifying the petrogenesis of syn-tectonic granitoids in the Wadi El-Sheikh area using petrographical and geochemical characteristics.

2. General geological setting of the investigated area.

The examined syn-tectonic granitoids, which are comparable to G1 Egyptian granites of [14] are represented in Wadi El-Sheikh region by quartz-diorite, tonalite and granodiorite. They surround Wadi El-Sheikh northern and southern flanks, which is a part of southern Sinai, Egypt Fig (1). The study area is delineated by the following co-ordinates: Latitudes 28°35` 00"and 28°52`00"N and Longitudes: 33°40` 00"

and 34°05` 00``E. The Syn-tectonic granitoids (the older granitoids) are characterized by slightly deformed, greenish grey to grey, medium-grained Fig (2), sometimes exhibited weak gneissose texture Fig (3). The syn tectonic granitoids generally form massive, grey masses with low to moderate relief, with medium to coarse granular texture. In some places older granitoids contain xenoliths of mafic (amphibolite), quartzo feldspathic rocks and calc-silicate which, have different shape and size where their amount increases toward the intrusion margin with the metagabbro. These xenoliths show a narrow reaction rim with the associated older granitoids. The xenoliths of amphibolite are most probably created as a result of assimilation process of the metagabbro- diorite rocks [19] Fig (5).

3. Petrography of the studied rocks

Based on the petrographic investigation of the studied SNG, they are classified into quartz- diorite, tonalite and granodiorite that can be described as follows.

3.1 Quartz-diorite

These quartz-diorite are medium- to coarse-grained, consisting essentially of plagioclase, quartz, hornblende, biotite, with few chlorite flakes and epidote (Fig. 6). Plagioclase ranges in composition from andesine to oligoclase. Quartz is coarse grained and scattered between crystals of plagioclase and mafic minerals. Hornblende is green to dark green and is frequently found with biotite, chlorite and opaque minerals. Sometimes the studied quartz-diorite exhibits a poikilitic texture Fig (8).

3.2 Tonalite

The studied tonalite has medium to coarse-grained texture, and is mostly composed of oligoclase, quartz, biotite, and hornblende (Fig. 9). Additionally, the gneissic texture of these rocks exhibits a parallel alignment of biotite and hornblende (Fig. 10). Plagioclase crystals ranges in composition from oligoclase to andesine which forms slightly altered subhedral to anhedral crystals. Quartz naturally arises as anhedral crystals that often occupy the spaces between other minerals and exhibit excessive extinction. Biotite has a basal cleavage and is often with a dark brown color. It forms as tiny flakes along the rock's foliation planes and is then changed into chlorite. Hornblende is green to dark green and is typically found with biotite, chlorite and opaque minerals.

3.3 Granodiorite

The studied granodiorite has a medium-grained hypidiomorphic texture and a grey to light pink color (Fig. 11). It consists mainly of plagioclase, quartz, with small amounts of potash feldspar, biotite, and hornblende. Some granodiorite is characterized by remarkable increase of biotite content (Fig 12&13).

4. Analytical methods

All samples were analyzed for their major, trace and rare earth element contents (REEs) tables (1&2). At Bureau VERITAS Commodities the Analytical Laboratories LDT, Canada, inductively coupled plasma-mass spectrometry (ICP-MS) was used to calculate the concentrations of main oxides, traces, and rare earth elements in the bulk samples. Additionally, the CIPW norm values are determined from the analytical data using the approach described by [20], and various statistical parameters are also calculated and listed in table (3). The geochemical characteristic of the three basic rock units presented in the region under consideration, is carried out through the examination of the chemical composition of (20) selected samples representing (8 samples from quartz-diorite, 4 samples from tonalite and 8 samples from granodiorite), at Wadi El-Sheikh.

5. Geochemistry

The collected data clearly demonstrate a decline in the abundance of SiO_2, K_2O, Rb, Zr and Hf from granodiorite to quartz diorite. The examined older granitoid exhibiting a wide range of silica contents from (52.43 - 71.49 Wt. %), being increased from quartz -diorite to granodiorite which is consistent with the acceleration of the differentiation of magma from quartz-diorite to granodiorite. Contrarily, there is an increase in the contents of CaO, MgO, Fe_2O_3 (t), TiO_2, Sr, Zn and V contents from granodiorite to quartz -diorite.

The analyzed samples of quartz-diorite and tonalite are chemically classified as tonalite, whereas those of granodiorite are classified as trondhjemite Fig (14a&14b). The Rb-Ba-Sr ternary discriminant diagram Fig (14c), reflected differentiation trend of

granitoid rocks from quartz diorite to granodiorite. the analyzed samples of SNG investigated that; the SNG comparable to the calc-alkaline older granitoids of Egypt Fig (14d). The investigated quartz diorite and gneissic tonalite are located in the line between tholeiitic and calc-alkaline, while granodiorite is pointed in calc-alkaline trend, being comparatively rich in total alkalis Fig (15a). [21] used the relation between Mol. [Al_2O_3/ ($CaO+Na_2O+K_2O$)] and Mol. [Al_2O_3/ (Na_2O+K_2O)] to discriminate between peralkaline, metaluminous and peraluminous types. On the diagram Fig (15b) the plots of the investigated granitoids are broadly distributed within the metaluminous field with markedly high A/NK values.

6. Tectonic setting

On the basis of Nb-SiO_2 diagram Fig (16a) stated by [22], the quartz-diorite, tonalite and granodiorite samples are pointed in volcanic- arc magma field. According to [22], "all igneous rocks with SiO_2 values that were formed above active Benioff zones have Nb contents below 15 ppm, whereas for granitic rocks products of within-plate continental magmatism with SiO_2 values between 60 and 75% have Nb lying in the range of 50 to 500 ppm. The studied granitic rocks have average Nb contents below 15 ppm. According to [23], in a subduction zone setting [24], the mantle above the descending oceanic lithosphere slab would be altered by low-Nb fluids and would not melt into acidic melts enriched in Nb. On the other hand, any magmatism of a within-plate variety could gradually enrich melts in Nb abundances". All of the current granitoids were produced above subduction zones, according to the aforementioned criteria. To differentiate between the tectonic settings of volcanic arc granites (VAG), syn-collision granites (Syn-COLG), oceanic ridge granites (ORG), and within plate granites (WPG), [25] presented a bivariate tectonic discrimination diagram. This diagram used the relation Rb (ppm) versus Y+Nb (ppm) in Fig (16b). Due to the low abundances of Rb, Nb, and Y in the studied granitoids, the data points mostly fall in the VAG field.

7. Depth of magma segregation

The CIPW normative compositions can be used as useful tools to present some data about the P-T conditions of granitic magma crystallization. The studied granitoids were produced in the pressure range of 0.5 to 10 kbar [26], as shown on the Ab-Q-Or ternary diagram of [27]. The studied granitoids have temperatures between 650°C and 700°C, according to the thermal lines [28] on the Ab-Q-Or ternary diagram. A binary relationship between Rb (ppm) and Sr (ppm) is proposed by [29] in Fig (17b) to calculate the crustal thickness, indicate that the studied granitoids have been created at greater depth more than 30 km of the lower crust. In general, the Egyptian granitoids' determined pressures [30&31] point to volcanic arc granitoids' deeper intrusion depths ('9-20Km) in comparison to post-collision granites' (5 Km). The OG's limited contact phenomena with the nearby rocks indicate that magma was deposited at a depth of about mid-crustal. The younger granites of the Egyptian basement are characterized by the shallow depths of emplacement of the post-collision granites [32, 33&34].

8. Evidence for magma mixing

The examined SNG exhibit high CaO/Na_2O ratios (0.33–1.44) that are decreasing from quartz-diorite to granodiorite (Table 1, Fig. 18a), as well as high Al_2O_3/TiO_2 ratios (17.85–80.70) that are increasing towards the higher silica granitic type (granodiorite). These characteristics show that the magma mixing of felsic and mafic melts had a significant impact on the emplacement of these granitoids. High-alumina granitoids can be created by melting a psammite (graywacke) source or by combining basaltic melt with granitic melt made from metapelites [35]. The high total contents of FeO*, MgO, and TiO_2 in the investigated OG support the mixing of mafic and felsic sources. These effects are most clearly visible in the variations of major oxide ratios, such as CaO/Na_2O and Al_2O_3/TiO_2, between mafic melts derived from the

mantle and crustal protoliths Fig (18a). The compositional points of the SNG members quartz-diorite, tonalite, and granodiorite are plotted close to the line of mixture melting of various compositions in the CaO/ Na_2O - Al_2O_3/TiO_2 and (FeO* + MgO + TiO_2). Additionally, all of the investigated SNG are distinguished by low Rb/Ba (0.05-0.21) and Rb/Sr (0.05-0.27) ratios, and their compositional locations are points in the field of sources depleted in clay minerals. Furthermore, the plots of Rb/Sr vs. Rb/Ba for the investigated SNG show a linear pattern of rising Rb/Sr with Rb/Ba (Fig. 18b), demonstrating

the impacts of variance in crustal contamination of mantle-derived basaltic magma.

9. Rare-Earth Elements (REE) concentrations.

The chondrite-normalized REE patterns are shown in Fig. 19, and REE together with statistical parameters are reported in Table (2). The fractionation between Light Rare-Earth Elements (LREE) and Heavy Rare-Earth Elements (HREE) is what distinguishes the REE patterns of all examined samples from the investigated SNG, shown in Fig. (19a). The high degree of fractionation, which increases from quartz-diorite [(La/Lu) N = 5.92-16.30] through tonalite [(La/Lu) N = 9.86-15.57] to granodiorite [(La/Lu) N =9.17-30.41], implies a significant amount of enrichment in the LREE compared to the HREE in all the examined SNG. Additionally, the majority of the OG samples under study exhibit concave-upward REE profiles as a result of the middle REE's (Gd to Er) relative depletion in comparison to the other HREE (Fig. 19a). The examined SNG are characterized by moderately fractionated HREE segments and little to no negative Eu anomalies Eu/Eu* (quartz-diorite (0.804-1.068)-tonalite (0.924-2.692) and granodiorite (0.639-0.811). According to the LREE, the investigated SNG Fig (19b) shows enrichment in the elements that are the least compatible with one another (such as Rb, Ba, and Th), and the enrichment factor decreases as the compatibility of the elements increases. Additionally, the examined SNG exhibit strong negative anomalies for the high-field-strength elements (HFSE; Tb, Tm, Nb, and Ta) as well as an overall enrichment in large ion lithophile elements (LILE; Rb, Ba, Th, Y, and K) in comparison to normalization values. The relative enrichment of the mantle source by the input of LILE from the dewatering slab is believed to be the cause of the HFSE depletion, which is a feature of subduction-related magmas and may be linked to crustal contamination [36]. Additionally, the examined SNG display notable negative P anomalies (Fig. 19b), which indicates the involvement of apatite and/or hornblende in the fractionating assemblages of granitic magma. Additionally, the examined SNG is distinguished by high abundances of trace elements that are incompatible with one another (LILE, HFSE), as well as by slightly negative Nb and Ta anomalies (Fig. 19b), which are not consistent with direct origination from crustal protoliths. The combined negative Nb-Ta and Zr-Hf anomalies seen in Fig (19b) indicate that the source of these granitoids was changed by subduction [37, 9, 38, 39, & 40].

10. Summary and conclusions

The field, petrography and geochemical investigation of the studied older granitoids, indicated that these granitoids are distinguished by quartz-diorite, tonalite and granodiorite. They are characterized by slightly deformed, greenish grey to grey, medium-grained sometimes with weak gneissose texture. Under the microscope, these quartz-diorite is medium to coarse grained, consisting mainly of plagioclase, quartz, hornblende and biotite, with few chlorite flakes and epidote. Tonalite is medium to coarse-grained, which are composed mainly of oligoclase, quartz, biotite, and hornblende. The granodiorite consists of plagioclase, quartz, with small amounts of potash feldspar, biotite, and hornblende in decreasing order of abundance. From geochemical data, we obtained that this granitoids are originated from calc-alkaline magma, metaluminous, and were created at moderate to high water pressure from (0.5 – 10) kbar and temperature of about 650ºC - 700ºC and formed at depth more than 30 km of the lower crust. The examined OG are distinguished by high abundances of trace elements that are incompatible with one another (LILE, HFSE). The studied older granitoids indicate the high CaO/Na_2O ratios (0.33-1.44) being decline from quartz-diorite to granodiorite, whereas they have also highly Al_2O_3/TiO_2 ratios from (17.85-80.70) increasing toward the higher silica granitic type (granodiorite). These characteristics show that the magma mixing of felsic and mafic melts had a significant impact on the emplacement of these granitoids.

.

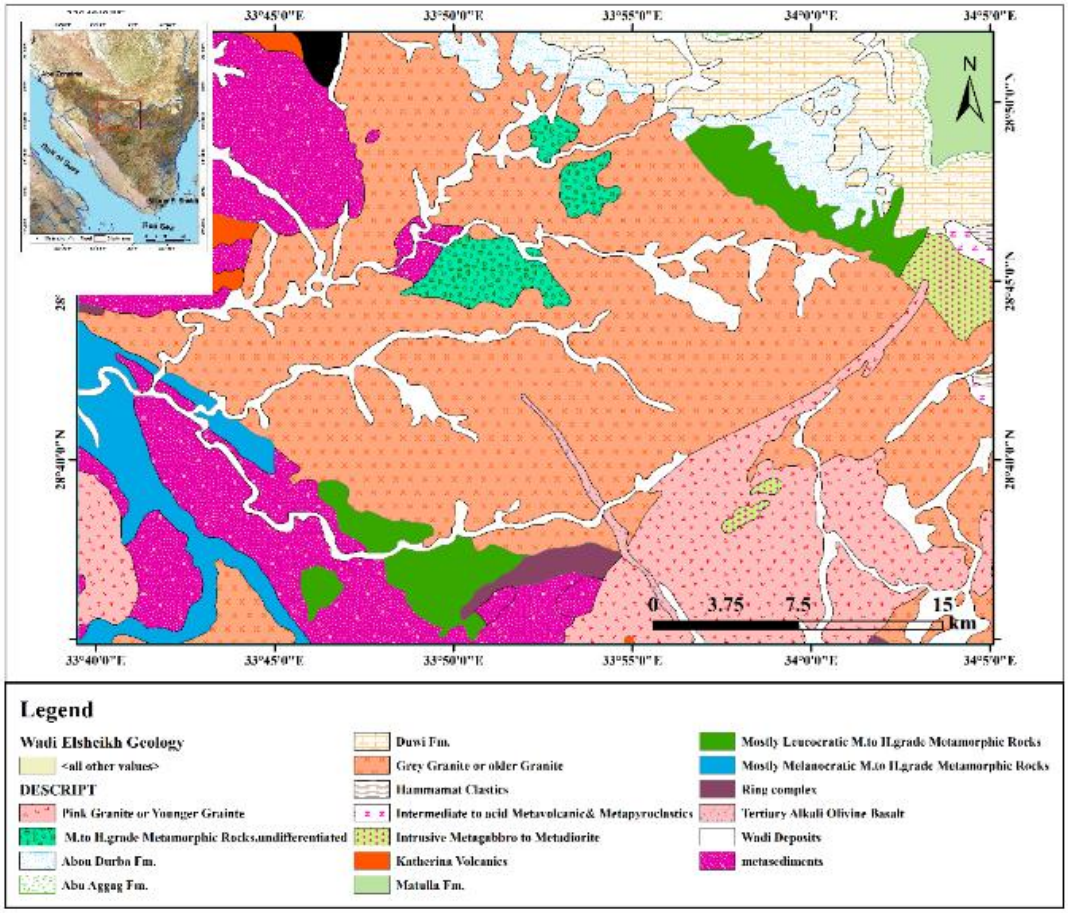

Fig (1): Geological map indicated the studied area (modified after [41]).

Fig (2): Photo show syn-tectonic granitoids (older granitoids) at Wadi El-Sheikh.

Fig (3): Photo show gneissosity in syn-tectonic granitoids (older granitoids) at Wadi El-Sheikh.

Fig (4): Photo show enclaves from amphibolite (Am) and calc-silicate (Calc) in syn-tectonic granitoids.

Fig (5): Photo show spindle-shaped xenolith of amphibolite (Am) within syn-tectonic granitoids (older granitoid) at Wadi El-Sheikh.

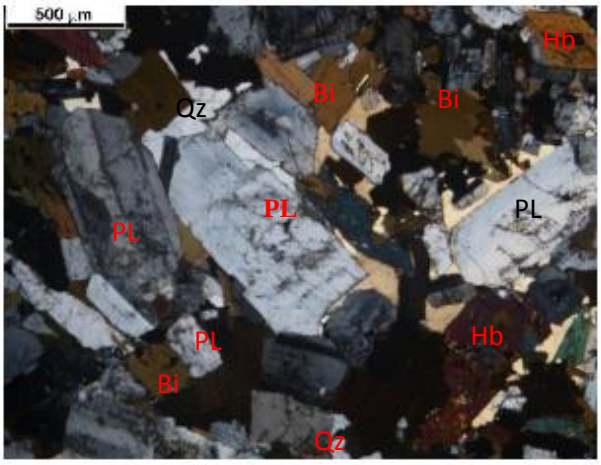

Fig (6) Photomicrograph showing mineral composition of quartz diorite. (X.P.L).

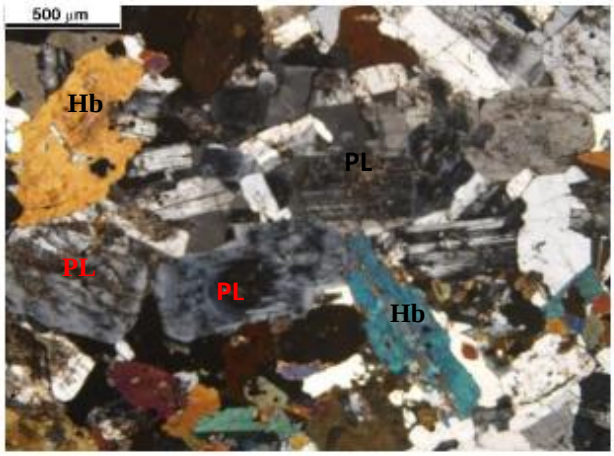

Fig (7) Photomicrograph showing zoned and highly altered plagioclase. (X.P.L).

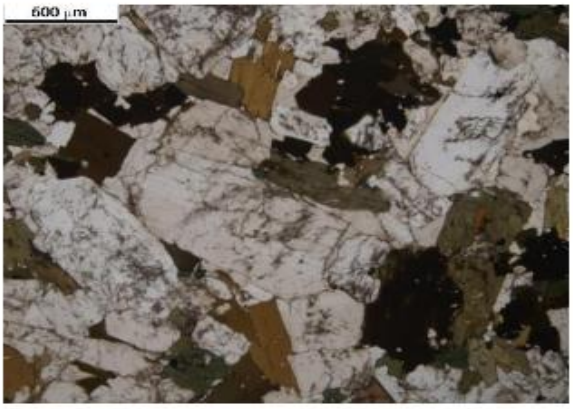

Fig (8) Photomicrograph showing poiklitic texture in quartz diorite. (P.P.L).

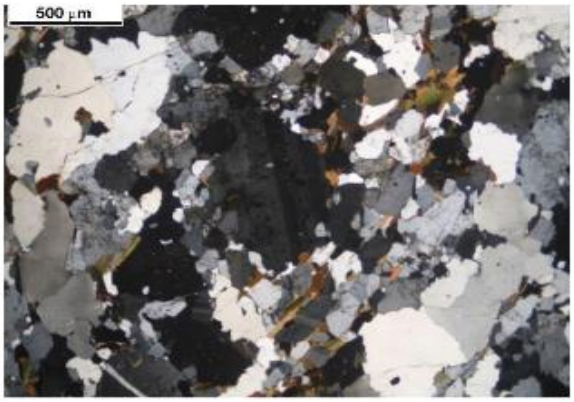

Fig (9) Photomicrograph showing mineral composition of gneissic tonalite. (X.P.L).

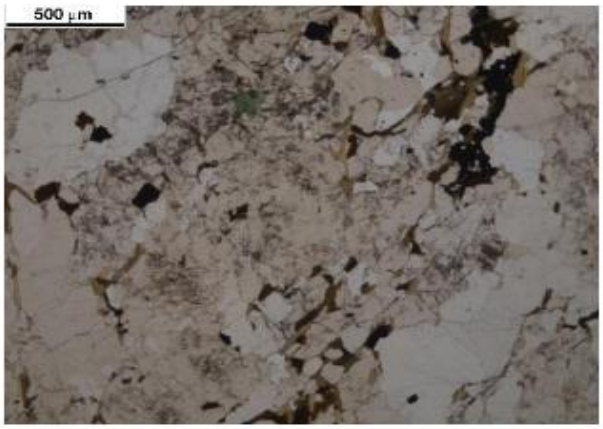

Fig (10) Photomicrograph showing gneissic texture in gneissic tonalite. (P.P.L).

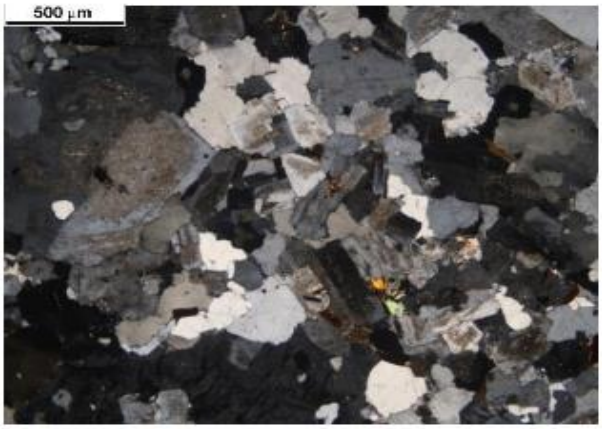

Fig (11) Photomicrograph showing subhedral granular texture of granodiorite. (X.P.L).

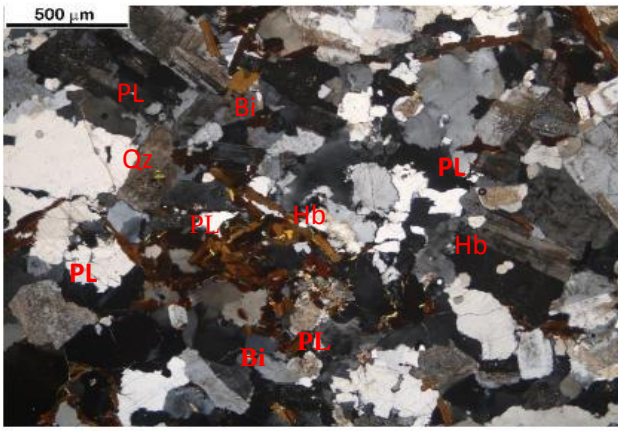

Fig (12) Photomicrograph showing mineral composition of biotite granodiorite. (X.P.L).

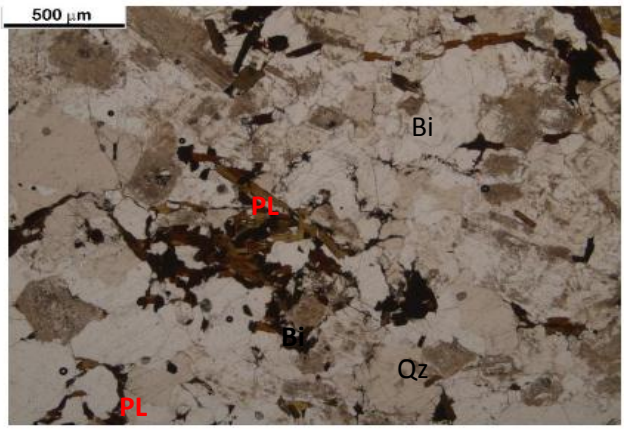

Fig (13) Photomicrograph showing mineral composition of biotite granodiorite. (P.P.L).

Table (1): Major oxide contents (in Wt.%) of the studied granitoids.

Rock Type	Quartz-diorite								Tonalite			
Sample No.	**kd 19**	**kd 21**	**SH 70**	**kd 32**	**kd 12**	**SH 51**	**kd 16**	**SH 40**	**SH 1`**	**b 1**	**SH 56**	**SH 69**
SiO_2	52.43	52.70	53.53	53.70	54.61	55.68	57.74	58.35	59.24	60.48	70.96	71.49
TiO_2	0.84	0.84	0.80	0.83	0.79	0.79	0.70	0.75	0.74	0.64	0.28	0.24
Al_2O_3	16.13	16.26	17.93	14.89	16.11	15.70	15.32	16.28	15.15	15.32	13.36	12.96
Fe_2O_3	6.85	6.51	5.86	6.28	5.91	6.01	5.05	5.06	4.85	4.13	2.23	1.79
FeO	6.16	5.85	5.27	5.65	5.31	5.40	4.54	4.55	4.36	3.72	2.01	1.61
MnO	0.11	0.11	0.10	0.12	0.10	0.10	0.09	0.10	0.11	0.07	0.04	0.03
MgO	3.90	3.66	1.97	3.66	3.10	3.35	2.49	1.64	2.14	2.29	0.65	0.50
CaO	5.96	5.67	5.33	5.65	4.87	4.98	4.39	3.69	4.04	3.82	2.84	2.59
Na_2O	4.15	4.19	4.81	4.26	4.18	3.90	4.09	4.73	4.60	4.39	4.14	4.17
K_2O	1.35	1.92	2.04	1.63	1.92	1.76	2.29	2.60	1.69	2.05	1.61	1.57
P_2O_5	0.25	0.25	0.31	0.26	0.24	0.23	0.22	0.24	0.23	0.22	0.14	0.06
L.O. I	1.87	2.05	2.05	3.08	2.86	2.11	3.09	1.99	2.85	2.88	1.75	3.01
Total	100	100	100	100	100	100	100	100	100	100	100	100
Na_2O+K_2O	5.50	6.10	6.85	5.89	6.10	5.66	6.38	7.34	6.29	6.44	5.76	5.74
CaO/Na_2O	1.44	1.35	1.11	1.33	1.16	1.28	1.08	0.78	0.88	0.87	0.69	0.62
Al_2O_3/TiO_2	19.19	19.39	22.44	17.85	20.38	19.94	21.92	21.65	20.41	24.11	48.23	53.95
FeO^t	12.32	11.71	10.55	11.29	10.63	10.81	9.08	9.11	8.72	7.44	4.01	3.22
Mol. $[Al_2O/(Na_2O+K_2O)]$	1.95	1.81	1.77	1.70	1.80	1.89	1.67	1.54	1.61	1.62	1.56	1.51
Mol. $[Al_2O/(CaO+Na_2O+K_2O)]$	0.84	0.84	0.91	0.78	0.90	0.90	0.89	0.94	0.90	0.93	0.97	0.98

Continued table (1): Major oxide contents (in Wt.%) of studied granitoids.

Rock Type	Granodiorite							
Sample No.	**SH 19**	**SH 12**	**SH 16**	**SH 14**	**SH 76**	**SH 77**	**SH 34**	**SH 73**
SiO_2	64.27	66.65	66.68	66.91	68.97	69.23	69.86	67.97
TiO_2	0.50	0.38	0.39	0.39	0.39	0.40	0.19	0.29
Al_2O_3	14.24	14.68	13.83	14.19	13.81	13.51	14.94	14.39
Fe_2O_3	3.83	2.77	2.77	2.82	2.30	2.60	1.37	2.27
FeO	3.45	2.49	2.49	2.53	2.07	2.34	1.23	2.04
MnO	0.07	0.06	0.05	0.06	0.05	0.05	0.02	0.05
MgO	1.67	0.80	1.04	0.96	0.73	0.80	0.36	0.56
CaO	3.57	2.57	2.64	2.71	2.20	2.41	1.82	2.18
Na_2O	3.91	4.89	4.18	4.49	4.04	4.49	5.44	4.36
K_2O	2.33	2.31	2.84	2.69	3.35	2.24	2.66	3.58
P_2O_5	0.15	0.09	0.10	0.09	0.13	0.15	0.06	0.13
L.O. I	1.99	2.3	2.97	2.16	1.97	1.78	2.05	2.16
Total	100	100	100	100	100	100	100	100
Na_2O+K_2O	6.24	7.20	7.02	7.17	7.39	6.73	8.10	7.94
CaO/Na_2O	0.91	0.53	0.63	0.60	0.54	0.54	0.33	0.50
Al_2O_3/TiO_2	28.27	38.94	35.73	36.50	35.84	33.46	80.70	49.03
FeO^t	6.89	4.99	4.99	5.07	4.14	4.68	2.47	4.09
Mol. $[Al_2O/(Na_2O+K_2O)]$	1.59	1.39	1.39	1.38	1.34	1.38	1.26	1.30
Mol. $[Al_2O/(CaO+Na_2O+K_2O)]$	0.92	0.96	0.94	0.93	0.97	0.95	0.99	0.96

Table (2): Trace and rare Earth Elements contents (ppm) of the studied older granitoids.

Rock Type	Quartz-diorite								Tonalite			
sample NO.	kd 19	kd 21	SH 70	kd 32	kd 12	SH 51	kd 16	SH 40	SH 1`	b 1	SH 56	SH 69
Rb	33.1	54.5	66.8	35.4	53.6	49.5	62.3	75.2	50.6	50.9	43.1	49.6
Ba	465	524	671	437	698	572	728	1016	517	520	455	337
Th	3	5.9	5.1	5.6	2.3	3.2	4.4	4.9	4.3	3.1	4.5	6.3
U	0.7	0.9	2.2	1	0.8	0.7	0.9	1.4	1.2	0.8	4.5	6.3
Nb	5.83	7.88	6.16	6.74	6.37	6.21	6.91	9.27	5.93	5.06	3.06	3.02
Ta	0.4	0.5	0.3	0.5	0.4	0.4	0.4	0.6	0.4	0.2	0.3	0.2
Zr	23.9	29.6	64.1	22.6	33	27.5	40	62.1	33.4	94.3	50.3	48.6
Pb	11.52	10.91	11.44	12.35	11.09	10.45	12.08	11.76	7.99	12.45	11.87	13.17
Y	16.5	19.3	12.1	16	17.6	17.9	16.5	18.4	13.2	9.3	6.1	2.3
Sr	627	605	810	583	594	580	539	601	686	685	529	478
La	19.5	31.4	18.8	17.1	20.4	20.4	22.8	21.7	21.6	19	15	14.4
Ce	41.27	61.73	37.84	38.37	43.62	44.47	48.55	45.33	47.16	38.21	27.27	24.05
Pr	4.8	6.5	4.4	4.6	5.3	5.4	5.5	5.2	5.9	4.2	2.7	2
Nd	20.2	25.2	18.4	22	22	22.1	22.2	21.2	22.8	17.6	9.7	6.4
Sm	4.1	4.8	3.6	4.7	4.5	4.4	4.2	4.5	4.1	3.7	1.5	0.8
Eu	1.2	1.2	1.2	1.4	1.2	1.2	1.1	1.3	1.2	1.2	0.8	0.6
Gd	3.6	4.1	3.1	4	3.8	3.8	3.6	3.9	3.2	2.8	1.1	0.5
Tb	0.4	0.5	0.3	0.5	0.4	0.5	0.4	0.5	0.4	0.3	0.1	0.1
Dy	2.9	3.4	2.3	3.5	3.2	3.2	3	3.3	2.4	2.4	1	0.3
Ho	0.6	0.6	0.4	0.6	0.6	0.6	0.6	0.6	0.4	0.4	0.2	0.1
Er	1.6	1.8	1.2	1.9	1.7	1.7	1.6	1.8	1.3	1.1	0.7	0.2
Tm	0.2	0.2	0.1	0.3	0.2	0.2	0.2	0.2	0.2	0.1	0.1	0.1
Yb	1.5	1.7	1	1.7	1.6	1.6	1.5	1.6	1.1	1	0.9	0.3
Lu	0.2	0.2	0.1	0.3	0.2	0.2	0.2	0.2	0.2	0.2	0.1	0.1
Rb/Sr	0.053	0.090	0.082	0.061	0.090	0.085	0.116	0.125	0.074	0.074	0.081	0.104
Rb/Ba	0.071	0.104	0.100	0.081	0.077	0.087	0.086	0.074	0.098	0.098	0.095	0.147
∑REEs	102.07	143.33	92.74	100.97	108.72	109.77	115.45	111.33	111.96	92.21	61.17	49.95
Eu/Eu*	0.931	0.804	1.068	0.959	0.861	0.873	0.841	0.924	0.974	1.091	1.814	2.692
La/Lu	10.12	16.30	19.51	5.92	10.59	10.59	11.83	11.26	11.21	9.86	15.57	14.95

Continued table (2): Trace and Rare Earth elements contents (ppm) of the studied older granitoids.

Rock Type	Granodiorite							
sample NO.	SH 19	SH 12	SH 16	SH 14	SH 76	SH 77	SH 34	SH 73
Rb	69.50	71.70	73.70	74.00	80.60	67.20	50.50	88.20
Ba	563.00	749.00	747.00	846.00	558.00	321.00	959.00	700.00
Th	8.00	8.90	10.00	7.20	8.70	11.10	2.00	10.00
U	1.40	1.90	1.70	1.10	2.00	2.20	1.00	2.10
Nb	4.95	6.52	5.24	5.29	7.25	7.84	2.02	6.33
Ta	0.50	0.60	0.40	0.40	0.70	0.70	0.20	0.70
Zr	38.50	50.10	45.20	42.50	64.20	79.40	115.90	75.70
Pb	9.27	9.71	8.87	9.37	15.94	14.73	16.04	17.51
Y	13.50	17.90	13.50	15.10	12.70	12.40	5.20	10.30
Sr	373.00	269.00	275.00	281.00	386.00	398.00	1,086.00	404.00
La	19.5	26.5	20.1	24	28.1	30.9	14.8	29.3
Ce	40.66	52.42	40.3	47.14	57.25	60.13	30.63	58.04
Pr	4.4	5.7	4.3	5.1	6.3	6.4	3.5	6.1
Nd	17	21.3	16.1	19.1	23.7	24.1	13.2	22.3
Sm	3.2	3.8	3	3.5	4.2	4.1	2.2	3.7
Eu	0.8	0.8	0.7	0.8	0.8	0.8	0.5	0.8
Gd	2.7	3.2	2.6	3	3.2	3.1	1.4	2.6
Tb	0.3	0.4	0.3	0.4	0.3	0.3	0.1	0.3
Dy	2.3	2.9	2.2	2.6	2.4	2.3	0.9	1.8
Ho	0.4	0.6	0.4	0.5	0.4	0.4	0.2	0.3
Er	1.3	1.7	1.3	1.5	1.2	1.2	0.5	0.9
Tm	0.2	0.2	0.2	0.2	0.2	0.2	0.1	0.1
Yb	1.3	1.8	1.3	1.4	1	1.2	0.6	0.9
Lu	0.2	0.3	0.2	0.2	0.1	0.2	0.1	0.1
Rb/Sr	0.186	0.267	0.268	0.263	0.209	0.169	0.047	0.218
Rb/Ba	0.123	0.096	0.099	0.087	0.144	0.209	0.053	0.126
∑REEs	94.26	121.62	93	109.44	129.15	135.33	68.73	127.24
Eu/Eu*	0.808	0.681	0.746	0.734	0.639	0.657	0.811	0.747
La/Lu	10.12	9.17	10.43	12.46	29.17	16.04	15.36	30.41

Table (3): CIPW norm of the studied older granitoids.

Rock Type	Quartz-diorite								Tonalite			
Sample No.	kd 19	kd 21	SH 70	kd 32	kd 12	SH 51	kd 16	SH 40	SH 1`	b 1	SH 56	SH 69
Quartz (Q)	4.64	3.62	3.26	6.10	7.52	10.15	12.06	10.03	14.07	15.29	33.39	34.69
Corundum(C)	0.00	0.00	0.00	0.00	0.00	0.00	0.00	0.00	0.00	0.00	0.00	0.00
Orthoclase (Or)	7.98	11.32	12.03	9.61	11.32	10.40	13.53	15.38	9.97	12.11	9.54	9.26
Albite (Ab)	35.09	35.43	40.70	36.06	35.39	33.02	34.57	40.06	38.95	37.17	35.05	35.29
Anorthite (An)	21.42	19.93	21.31	16.68	19.53	20.12	16.70	15.49	15.69	16.03	13.08	12.01
Plagioclase (PL)	56.50	55.35	62.01	52.74	54.93	53.14	51.27	55.55	54.64	53.20	48.13	47.30
Diopside wo	2.73	2.75	1.30	4.04	1.27	1.29	1.52	0.53	1.20	0.62	0.05	0.19
Diopside en	1.74	1.76	0.71	2.61	0.80	0.83	0.95	0.29	0.73	0.40	0.03	0.10
Dioside fs	0.80	0.81	0.54	1.15	0.39	0.38	0.48	0.22	0.41	0.18	0.02	0.09
Diopside (Di)	5.28	5.32	2.56	7.81	2.47	2.50	2.96	1.05	2.34	1.20	0.11	0.38
Hypersthene en	7.96	7.37	4.20	6.51	6.92	7.52	5.25	3.80	4.60	5.30	1.58	1.14
Hypersthene fs	3.67	3.38	3.16	2.87	3.36	3.46	2.69	2.89	2.57	2.32	1.43	1.04
Hypersthene (Hy)	11.63	10.74	7.36	9.38	10.28	10.98	7.94	6.69	7.17	7.61	3.01	2.18
Magnetite (Mt)	9.93	9.43	8.50	9.10	8.56	8.71	7.32	7.34	7.03	5.99	3.23	2.59
Ilmenite (Il)	1.60	1.59	1.52	1.58	1.50	1.50	1.33	1.43	1.41	1.21	0.53	0.46
Apatite (Ap)	0.57	0.57	0.72	0.60	0.56	0.53	0.52	0.55	0.53	0.51	0.31	0.13
Total	98.14	97.96	97.95	96.93	97.15	97.90	96.92	98.01	97.15	97.12	98.25	96.99

Continued table (3): CIPW norm of the studied older granitoids.

Rock Type	Granodiorite							
Sample No.	**SH 19**	**SH 12**	**SH 16**	**SH 14**	**SH 76**	**SH 77**	**SH 34**	**SH 73**
Quartz (Q)	22.26	22.30	24.18	23.20	26.70	28.07	23.40	23.25
Corundum(C)	0.00	0.00	0.00	0.00	0.00	0.00	0.00	0.00
Orthoclase (Or)	13.74	13.67	16.81	15.88	19.80	13.25	15.74	21.15
Albite (Ab)	33.12	41.37	35.34	37.96	34.17	38.02	46.00	36.92
Anorthite (An)	14.42	11.27	10.58	10.63	9.66	10.07	8.50	9.12
Plagioclase (PL)	47.55	52.64	45.92	48.60	43.83	48.08	54.50	46.04
Diopside wo	0.95	0.38	0.78	0.93	0.16	0.37	0.06	0.37
Diopside en	0.57	0.19	0.45	0.51	0.09	0.20	0.03	0.18
Dioside fs	0.33	0.17	0.30	0.38	0.07	0.16	0.03	0.19
Diopside (Di)	1.85	0.75	1.53	1.82	0.32	0.73	0.12	0.73
Hypersthene en	3.61	1.79	2.15	1.89	1.73	1.78	0.88	1.23
Hypersthene fs	2.13	1.61	1.45	1.42	1.29	1.42	0.83	1.29
Hypersthene (Hy)	5.74	3.40	3.60	3.31	3.02	3.20	1.71	2.52
Magnetite (Mt)	5.56	4.02	4.02	4.08	3.34	3.77	1.99	3.30
Ilmenite (Il)	0.96	0.72	0.74	0.74	0.73	0.77	0.35	0.56
Apatite (Ap)	0.36	0.21	0.23	0.22	0.30	0.35	0.13	0.29
Total	98.01	97.70	97.03	97.84	98.03	98.22	97.95	97.84

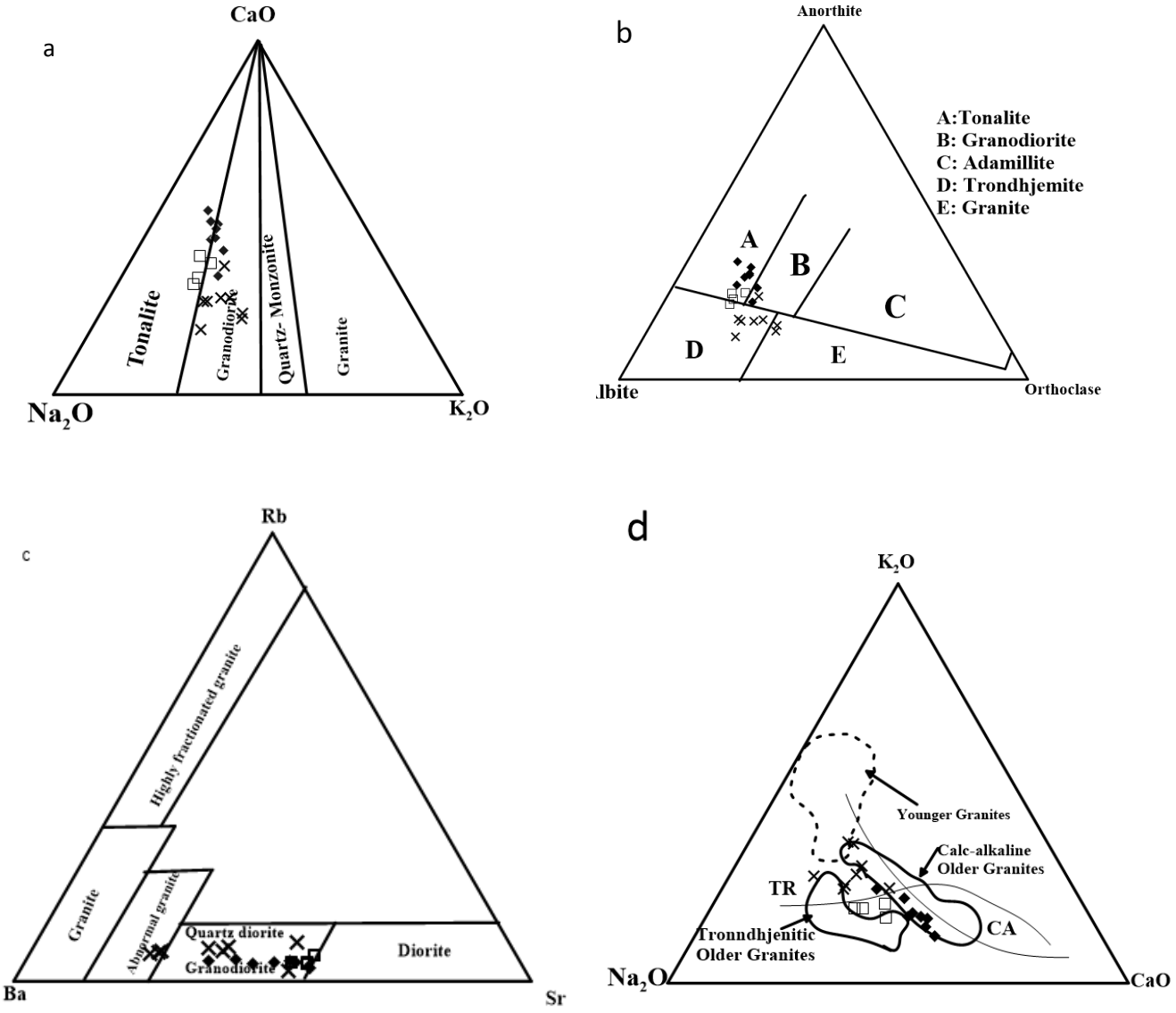

Fig (14): (a) Na_2O-CaO-K_2O diagram for nomenclature of the OG after [42], (b) the Rb-Ba-Sr ternary discriminant diagram [43], (c) ternary plot of normative content (Ab-An-Or) for the studied granitoids, the classification boundaries after [44] and classified diagram of the granitoid rocks of Egypt after [32], trondhjemitic (TR)and calc-alkaline (CA) trends are from [45]. Symbol in Figs (14-19): (♦) quartz diorite, (□) tonalite and (×) granodiorite.

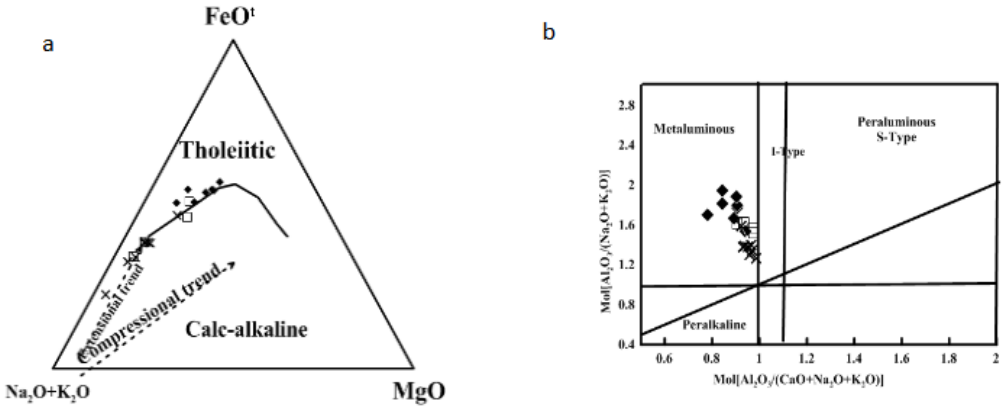

Fig (15): (a) the AFM ternary diagram for the examined granitoids, after [46]. The compressional and extensional trend after [47], (b) variation of Shand's index for the investigated granitoids, after [48]. I-type and s-type boundary after [21].

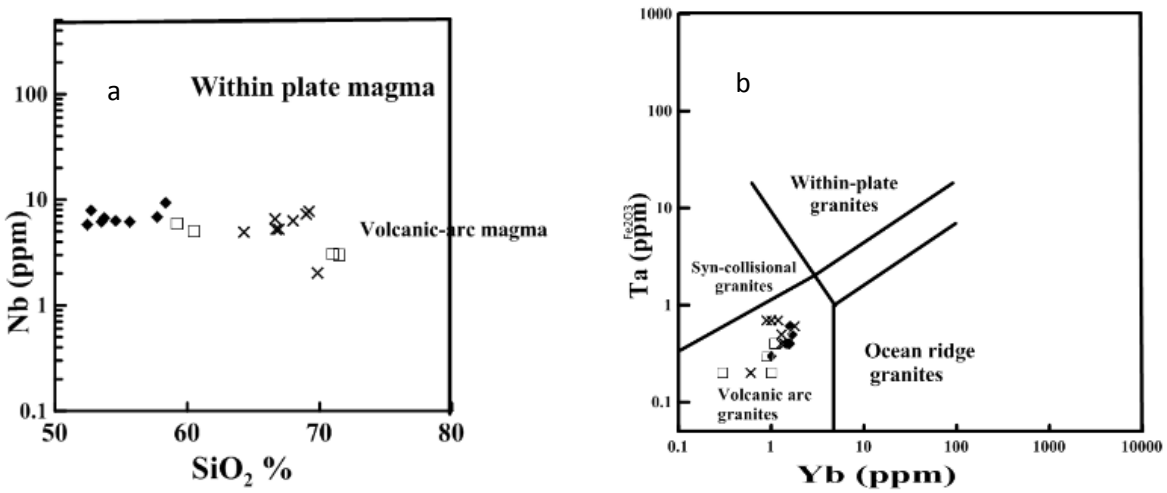

Fig (16): (a) Nb verses SiO_2 diagram for the investigated granitoids. Fields, after [22], and (b) Rb vs. (Y+Nb) discrimination diagram for the studied granitoids, after [25].

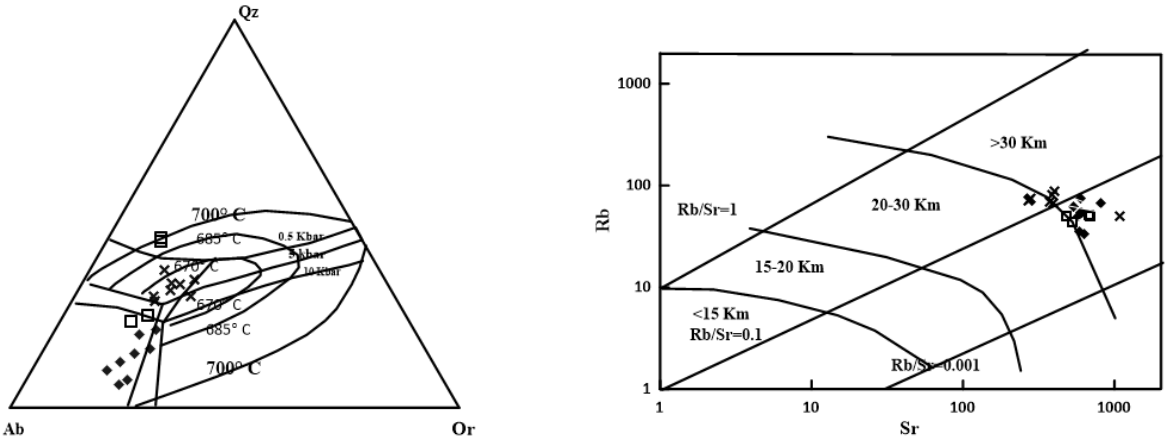

Fig (17): (a) normative Ab-Qz-Or diagram for the studied granitoids. Solid lines represent 0.5 and 10 Kbar pH_2O, after [27]. Dotted lines represent the trace of isobaric minimum of eutectic points at intermediate water vapor pressure, and (b) plotting of the studied granitoids on Sr (ppm) vs. Rb (ppm) binary diagram. The dashed lines refer to the crustal thickness, after [29].

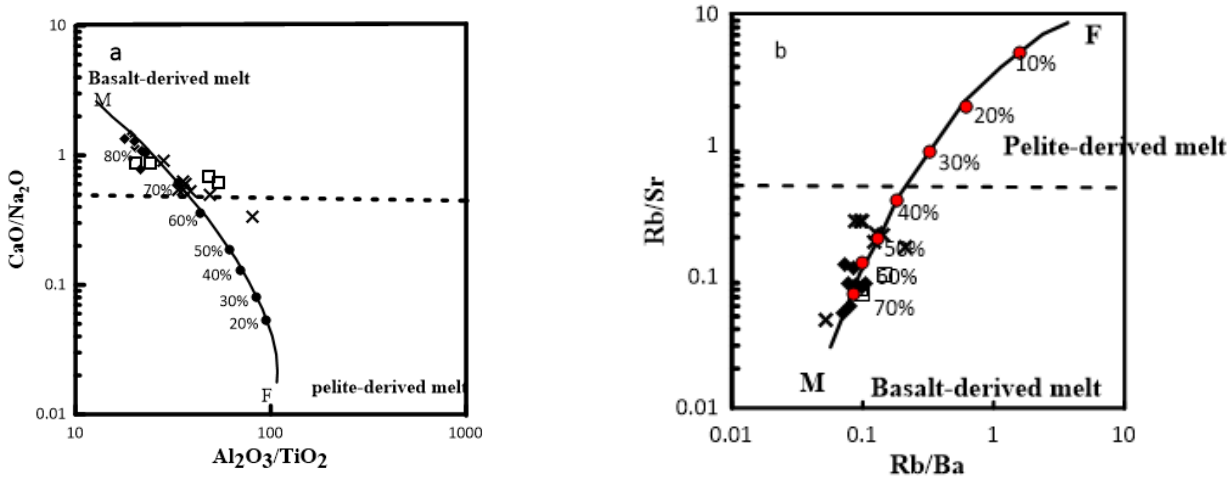

Fig (18): (a) CaO/Na_2O vs. Al_2O_3/TiO_2 diagram [35] for the examined OG. Between Phanerozoic basalt [49] (point M "mafic") and melt formed from crustal melt is considered as the 850 o C, 10 kbar crust-derived (experimental) melt (Point F "Felsic") following [50]. This line was computed to represent the mixing of basaltic and granitic melts. (b) Rb/Ba verses Rb/Sr diagram for the examined OG. End-member compositions for mafic and felsic melt are the same as in Fig (18a).

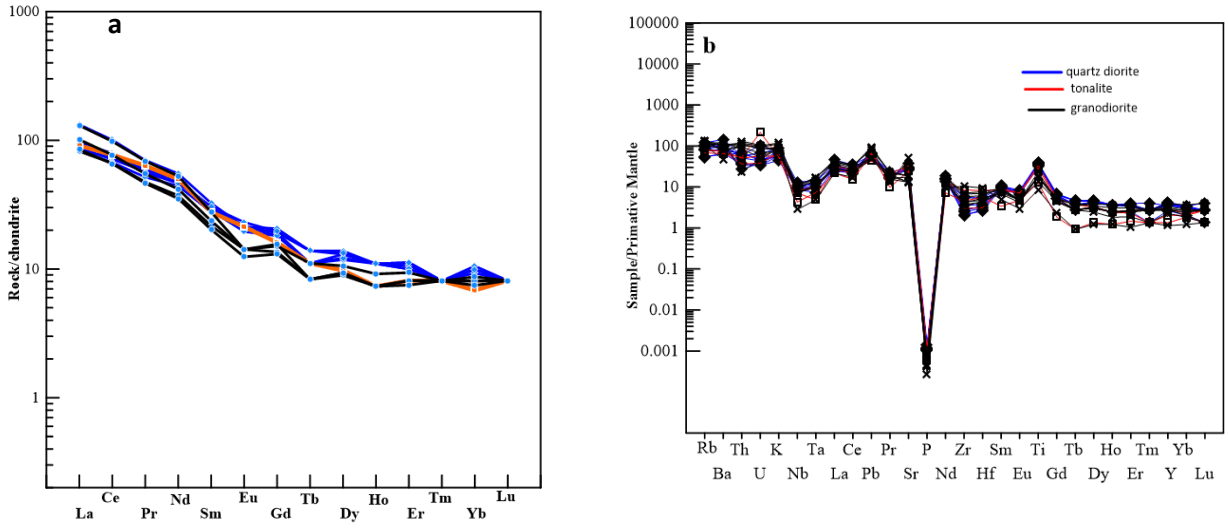

Fig (19): (a) Chondrite-normalized REE patterns for the examined OG. Normalizing values are from [51]. (b) N-MORB normalized multi-element patterns of trace elements in the examined OG. N-MORB concentrations from [51].

11. References

[1] Be'eri-Shlevin Y, Katzir Y, Whitehouse MJ, Kleinhanns IC (2009) Contribution of pre Pan-African crust to formation of the Arabian Nubian Shield: new secondary ionization mass spectrometry U-Pb and O studies of zircon. Geol. 37(10):899–902.

[2] Johnson PR, Andresen A, Collins AS, Fowler AR, Fritz H, Ghebreab W, Kusky T, Stern RJ (2011) Late Cryogenian-Ediacaran history of the Arabian-Nubian Shield: a review of depositional, plutonic, structur-al, and tectonic events in the closing stages of the northern East african Orogen. J Afr Earth Sci 61:167–232.

[3] Fritz H, Abdelsalam M, Ali KA, Bingen B, Collins AS, Fowler AR, Ghebreab W, Hauzenberger CA, Johnson PR, Kusky TM, Macey P, Muhongo S, Stern RJ, Viola G (2013) Orogen styles in the East African Orogen: a review of the Neoproterozoic to Cambrian tectonic evolution. J Afr Earth Sci 86:65–106.

[4] Be'eri-Shlevin Y, Eyal M, Eyal Y, Whitehouse MJ, Litvinovsky B (2012). The Sa'al volcano-sedimentary complex (Sinai, Egypt): a latest Mesoproterozoic volcanic arc in the northern Arabian Nubian Shield. Geology 40:403–406.

[5] Johnson PR, Halverson GP, Kusky TM, Stern RJ, Pease V (2013). Volcano sedimentary basins in the Arabian-Nubian Shield: markersof repeated exhumation and denudation in a Neoproterozoic Accretionary Orogen. Geosciences 3(3):389–445.

[6] Oriolo S, Oyhantçabal P, Wemmer K, Siegesmund S (2017) Contemporaneous assembly of Western Gondwana and finalRodinia break-up: implications for the

supercontinent cycle. Geosci Front 8:1431–1445.

[7] Jackson N.J., Walsh J.N., and Pegram E. (1984) Geology, geochemistry and petrogenesis of Late Precambrian granitoids in the Central Hijas region of the Arabian Shield [J]. Contr. Mineral. Petrol. 87, 205–219.

[8] Garfunkel Z (1999) History and paleogeography during the Pan-African orogen to stable platform transition: reappraisal of the evidence from the Elat area and the northern Arabian–Nubian Shield. Israeli J Earth Sci 48:135–157.

[9] Jarrar GH, Manton WI, Stern RJ, Zachmann D (2008) Late Neoproterozoic A-type granites in the northernmost Arabian- Nubian Shield formed by fractionation of basaltic melts. Chemie der Erde – Geochemistry 68:295–312.

[10] Azer, M.K. (2013): Late Ediacaran (605–580 Ma) post-collisional alkaline magmatism in the Arabian–Nubian Shield: a case study of Serbal ring-shaped intrusion, southern Sinai, Egypt. J. Asian Earth Sci., 77, 203-223.

[11] Jarrar GH, Stern RJ, Saffarini G, Al-Zubi H (2003) Late and post- orogenic Neoproterozoic intrusions of Jordan. Implications for crustal growth in the northernmost segment of the East African orogeny. Precambrian Res 123:295–320.

[12] Moussa, E.M.M., Stern, R.J., Manton, W.I., and Ali, K.A., 2008, SHRIMP zircon dating and Sm/Nd isotopic investigations of Neoproterozoic granitoids, Eastern Desert, Egypt: Precambrian Research, v. 160, p. 341–356. doi:10.1016/j. precamres.2007.08.006.

[13] Stern, R.J. and Hedge C.E. (1985): Geochronologic and isotopic constraints on late Precambrian crustal evolution in the Eastern Desert of Egypt. Am. J. Sci., 285, 97-127

[14] Hussein, A. A., Ali, M. M., and El Ramly, M. F., 1982. A proposed new classification of the granites of Egypt.: J. Volcan. & Geoth. Research, v. 14, p. 187-198.

[15] Gass, I. G., 1977. The evolution of the Pan-African crystalline basement in NE Africa and Arabia. J. Geol. Soc. London 134. 129-138.

[16] Bentor YK (1985) The crustal evolution of the Arabo-Nubian Massif with special reference to the Sinai Peninsula. Precambrian Res 28:1–74.

[17] Abdel-Karim AM, Arva-Sos E (1992) Geology and K-Ar ages of some older and younger granites in Southwestern Sinai, Egypt. Proc. 3rd Conf. Geol. Sinai Develop., Ismailia 261–266.

[18] Abdel-Karim AM (1995) Late Precambrian metagabbro-diorite complex from Southwest Sinai, Egypt. Egypt J Geol 39:215–238.

[19] Soliman, F. A. and Hassen, I. S., 1999, Geochemical typology and origin of the granitoid rocks of Wadi Akhdar, Central-South Sinai. Acta Mineralogica-Petrographica, Szeged, XL: 105-120.

[20] Kelsey (1965). Calculation of the C.I.P.W. norm. Mineralogical magazine, v. 34, p. 276-282.

[21] Maniar, P.D., Piccoli P.M. (1989): Tectonic discrimination of granitoids. Geol. Soc. Am. Bull., 101, 635-643

[22] Pearce, J. A., and Gale, G. H., 1977. Identification of ore-deposition environment from trace element geochemistry of associated igneous host rocks: Geological Society of London Special Publication, v. 7, p. 14-24.

[23] Gass, I. G., 1979. Evolutionary model for the Pan-African crystalline basement: I. A.G. Bull., (Jeddah), v. 3, p. 11-20.

[24] Ringwood, A. E., 1974. The petrological evolution of island arc systems. Journal Geological Society London 130, 183-204.

[25] Pearce, J. A., Harris, N. B. W., and Tindle, A. G., 1984. Trace elements discrimination diagrams for the tectonic interpretation of granitic rocks. J. Petrol., v. 25, pp. 956-983.

[26] Luth, W. C., Jams, R. H. and Tuttle, O. F., 1964. The granite system at pressure of 4 to 10 kilobars. J. Geophys. Res., 69, 759-773.

[27] Tuttle, O. F. & Bowen, N. L., 1958. Origin of granite in the light of experimental studies in the system $NaAlSi_3O_8$-$KAlSi_3O_8$-SiO_3-H_2O, Geological Society America Memoir, 74, 1-153.

[28] James, R.S. & Hamilton, D.L. (1969): Phase relations in the system $NaAlSi_3O_8$-$KAlSi_3O_8$-$CaAl_2Si_2O_8$-SiO_2 at 1 kilobar water vapour pressure. Contrib Mineral. Petrol., 21, 111–141.

[29] Condie KC (1973) Archean magmatism and crustal thickening. Geol Soc Am Bull 84:2981–2991

[30] Farahat ES, El-Mahalawi MM, Hoinkes G (2004) Continental back-arc basin origin of some ophiolites from the Eastern Desert of Egypt. Mineral Petrol 82:81–104

[31] Helmy H, Kaindl R, Fritz H, Loizenbauer J (2004) The Sukari Gold Mine, Eastern Desert, Egypt: structural setting, mineralogy and fluid inclusion study. Miner Deposita 39:495–511

[32] Hassan, M.A., Hashad, A.H., 1990. Precambrian of Egypt. In: Said, R. (Ed.), The Geology of Egypt. Balkema, Rotterdam, pp. 201–245.

[33] Abdel Aal, A., 1996. Proterozoic A-type granite: a study from the northeastern Nubian Shield, Egypt. Egyptian Journal of Geology, 40: 631-659.

[34] Farahat ES, Mohamed HA, Ahmed AF, El Mahallawi MM (2007) Origin of I- and A-type granites from the Eastern Desert of Egypt: Implications for crustal growth in the northern Arabian-Nubian Shield. J Afr Earth Sc 49:43–58.

[35] Sylvester PJ (1989) Post-collisional alkaline granites. J Geol 97: 261–280.

[36] McCulloch, M.T., Gamble J. (1991): Geochemical and geodynamical constraints on subduction zone magmatism. Earth Planet. Sci. Lett., 102, 358-374.

[37] Beyth, M., Stern R.J., Altherr R., Kröner A. (1994): The late Precambrian Timna igneous complex, southern Israel: evidence for comagmatic-type sanukitoid monzodiorite and alkali granite magma. Lithos. 31, 103-124.

[38] Kessel, R., Stein M., Navon O. (1998): Petrogenesis of Late Neoproterozoic dikes in the Northern Arabian–Nubian Shield: implications for the origin of A-type granites. Precambrian Res., 92, 195-213.

[39] Mushkin, A., Navon O., Halicz L., Hartmann G., Stein M. (2003): The petrogenesis of A- type magmas from the Amram Massif, southern Israel. J. Petrol., 44, 815-832.

[40] Stern, R.J., Voegeli D.A. (1987): Geochemistry, geochronology, and petrogenesis of a Late Precambrian (~ 590 Ma) composite dike from the North Eastern Desert of Egypt. Geol. Rundsch., 76, 325-341.

[41] Conoco (Continental Oil Company) (1987) Geological map of Egypt (scale 1:500000). Conoco Inc. in collaboration with Freie University at Berlin, Ponca City.

[42] Hunter, D. R., Barker, F., and Millard, H. T., 1978. The geochemical nature of the Archean ancient gneiss complex and granodiorite suite, Swaizland: A preliminary study: Precambrian Res., v. 7, p. 105-127.

[43] El Bouseily, A.M. and El Sokkary, A.A. (1975) The Relation between Rb, Ba and Sr in Granitic Rocks. Chemical Geology, 16, 207-219.

[44] Barker, F., 1979. Trondhjemites, dacites and related rocks. Amsterdam, Elsevier, 414 p.

[45] Barker, F., Arth J.G. (1976): Generation of trondhjemitic-tonalitic liquids and Archean bimodal trondhjemite-basalt suites. Geology. 4, 596-600.

[46] T. N. Irvine, and W. R. A. Baragar, A guide to chemical classification of the common volcanic rocks. Canada: J. Earth Sci., Vol. 8, pp. 523-548, 1971.

[47] Pearce, J.A., Norry M.J. (1979): Petrogenetic implications of Ti, Zr, Y, and Nb variations in volcanic rocks. Contrib. Mineral. Petrol., 69, 33-47.

[48] Shand, S. J., 1927. Eruptive Rocks: Thomas Murby and Co; London., P.488.

[49] Condie, K.C. (1993): Chemical composition and evolution of the upper continental crust: contrasting results from surface samples and shales. Chem. Geol., 104, 1-37.

[50] Patiño Douce, A.E., Johnston A.D. (1991): Phase equilibria and melt productivity in the pelitic system: implications for the origin of peraluminous granitoids and aluminous granulites. Contrib. Mineral. Petrol., 107, 202-218.

[51] Sun, S.-S., McDonough W. (1989): Chemical and isotopic systematics of oceanic basalts: implications for mantle composition and processes. Geol. Soc. Lon. Spec. Pub., 42, 313-345